

# Compositional Pore-Network Modeling of Gas-Condensate Flow: Effects of Interfacial Tension and Flow Velocity

P. K. P. Reis, M. S. Carvalho\*

*Department of Mechanical Engineering, Pontifícia Universidade Católica do Rio de Janeiro, Rio de Janeiro-RJ 22451-900, Brazil*

---

## Abstract

Liquid dropout and retention in gas-condensate reservoirs, specially in the near wellbore region, obstruct gas flowing paths and impact negatively the produced fluid volume and composition. Yet, condensate banking forecasting is commonly inaccurate, as experiments seldom reproduce reservoir extreme conditions and complex fluid composition, while most pore-scale models oversimplify the physics of phase transitions between gas and condensate. To address this gap, a fully implicit isothermal compositional pore-network model for gas and condensate flow is presented. The proposed pore-networks consist of 3D structures of pores connected by constricted circular capillaries. Hydraulic conductances are calculated for the capillaries, which can exhibit single-phase flow or two-phase annular flow, according to local gas and liquid saturations, or be blocked by a liquid bridge, when capillary forces overcome viscous forces. A PT-flash based on the Peng-Robinson EoS is performed at control volumes defined for the pores at each time step, updating the phases properties. Flow analyses were carried based on coreflooding experiments reported in the literature, with matching fluid composition and flow conditions, and approximated pore-space geometry. Predicted and measured relative permeability curves showed good quantitative agreement, for two values of interfacial tension and three values of gas flow velocity.

*Keywords:* Gas Condensate Relative Permeabilities, Dynamic

---

\*Corresponding author

*Email addresses:* paulareis@lmpm.mec.puc-rio.br (P. K. P. Reis), msc@puc-rio.br (M. S. Carvalho )

## 1. Introduction

Hydrocarbon recovery from gas condensate reservoirs tends to undergo a sharp decline in the event of condensate banking (El-Banbi et al., 2000; Barnum et al., 1995). As the near wellbore region is depleted below the gas dew point pressure, retrograde condensation occurs, leading to a subsurface liquid saturation buildup. Consequently, not only the gas flow rate is significantly hindered, but valuable heavier components are trapped in the porous medium, leading to a leaner produced gas.

In order to prevent low productivity and promote economic viability in gas condensate field developments, several production optimization and EOR methods have been proposed recently (Azin et al., 2019; Davarpanah et al., 2019; Hoseinpour et al., 2019; Mazarei et al., 2019; Zhang et al., 2020). These methods commonly involve the injection of gas ( $CO_2$ ,  $N_2$ ,  $CH_4$ ,  $C_2H_6$  and re-injected gas) to alter phase behavior and sustain reservoir pressure, and the injection of wettability modifier chemicals to alter rock surfaces from condensate-and water-wet to preferentially gas-wet. Adequate development of such production enhancement schemes requires deep understanding of the coupled flow of gas and condensate in porous media and its dependency on parameters like flow rate, phases properties, pore morphology and wettability, which has been proved to be fundamentally different from that observed in conventional two-phase flow systems (Jamiolahmady et al., 2003b).

To this end, coreflooding experiments have been widely used and provided relevant macro-scale data, such as critical condensate saturation ( $S_{cc}$ ) and relative permeability curves, as well as their dependency on interfacial tension and flow rate. (Chen et al., 1995; Henderson et al., 1998; Jamiolahmady et al., 2003a; Mott et al., 2000). Additionally, visualization of gas and condensate flow in micromodels contributed with valuable qualitative data regarding flow patterns, phase change and phase trapping in pores (Al Harasi et al., 2009; Coşkuner, 1997; Dawe and Grattoni, 2007). However, due to experimental operation constraints, these experiments seldom reproduce extreme pressure and temperature conditions or use complex fluid compositions normally occurring in gas condensate reservoirs. This leads to significant uncertainties in results, since model fluids do not always accurately capture the flow characteristics of compositionally complex reservoir fluids and may not mimic the reservoir wettability (Nagarajan et al., 2004).

As an alternative, similar data can be obtained via pore-scale modeling (Blunt et al., 2013). Pore-network models of multiphase flow could be particularly suitable for this purpose, as they have shown promising results for predictive purposes, while being computationally less demanding than direct models (Joekar-Niasar and Hassanizadeh, 2012). In the past decades extensive research effort has been directed to the development of this class of simulation tools, with a few regarding specifically gas and condensate flow. An overview of the works available in the literature concerning pore-network modeling of gas and condensate flow is presented next.

Mohammadi et al. (1990) represented the pore space as Bethe trees and calculated relative permeabilities using percolation theory. Threshold radii as a function of pressure were defined to determine which capillaries were filled with liquid. Also, condensate accumulation in tight corners was considered by adopting capillaries with convex polyhedral cross sections. Relative permeabilities showed sensitivity to pore geometry, connectivity and size distribution. Fang et al. (1996) developed a phenomenological model to calculate condensate critical saturation and its dependency on interfacial tension and contact angle hysteresis. Their model contemplated only gravitational and capillary forces and the network was composed of cylindrical capillaries. At each time step, a finite amount of condensate was arbitrarily added to the capillaries with radii below the threshold radius of  $20\mu m$ . Critical condensate saturation increased as interfacial tension rose and it was also affected by contact angle hysteresis. Wang and Mohanty (1999) also developed a model for  $S_{cc}$  determination. They used a 3D pore-network with converging-diverging pore throats, with square cross section, so that liquid accumulation in the corners was assessed. Condensation in the pore throats was also associated with their radii. Under gravitational and capillary forces, they have observed that  $S_{cc}$  increased with interfacial tension and decreased with connate water saturation. The same authors upgraded their model by including viscous forces and relative permeability calculations (Wang et al., 2000). In this work, two scenarios were analyzed: low capillary number regime and low condensate saturation/high pressure gradient flow regime. In the first, relative permeabilities were strongly sensitive to the pore structure. In the second, both gas and condensate relative permeabilities increased with their saturation and pressure gradient. Li et al. (2000) also included viscous forces in a model based on Fang et al. (1996) and calculated both  $S_{cc}$  and relative permeabilities. They have concluded that the effect of gravity and viscous forces in the  $S_{cc}$  is significant especially at low

interfacial tension, but that the most relevant parameter is wettability. As for the relative permeabilities, interfacial tension and viscous forces are important parameters, which is in line with experimental data. Jamiolahmady et al. (2000) developed a mechanistic model for gas and condensate flow in a single pore throat to describe the rate effect on relative permeabilities. In this model, both phases are injected in a conical pore and the fluid spacial distribution is controlled by an evolution equation that describes the condensate film position, used when the flow is annular, and a gas advancement equation, used when a bridge of condensate is formed. The positive effect of flow rate on the gas relative permeability was more pronounced than that on the condensate relative permeability, while a decrease in interfacial tension led to a increase in the permeabilities of both phases. The same authors also developed a 3D pore-network model and compared results with coreflooding experiments (Jamiolahmady et al., 2003b). The network was composed of cylindrical capillaries and the evolution equation (Jamiolahmady et al., 2000) was replaced by a simpler evolution time correlation. The predicted values were not quantitatively equivalent to the corresponding measured ones, but the rate sensitivity of the relative permeabilities was similar to the measured data. Bustos and Toledo (2003) developed a mechanistic model with 2D and 3D networks of capillaries with square cross section. Similarly to Fang et al. (1996), condensation happened in discrete steps, but in this case it started at the capillary corners before evolving into a condensate bridge. Viscous forces were not included and relative permeability, notably for the gas, was sensitive to geometric parameters.

Those works have in common the shortcoming of not reproducing the effects of phase equilibrium thermodynamics on gas and condensate coupled flow. Important phenomena like the accumulation of heavier hydrocarbons in the porous media or the dependency of interfacial tension and saturation on pressure are not appraised. In order to address this issue, Momeni et al. (2017), have proposed a compositional 3D pore-network model for dynamic displacement of gas and condensate in wellbore region. In their model, a flash calculation is performed at each throat at every time step, determining the phases properties and saturations. Square capillaries were used and two fluid configurations were allowed: gas core with condensate flowing in the corners or a fully saturated throat by condensate. The pores were considered to be volumeless and impose no restriction to flow, while the throats conductances were calculated with Poiseuille law with no slip boundary condition at the solid-fluid interfaces and free slip at the fluid-fluid interfaces. Fluids were

injected at the inlet at fixed flow rate and separated mass balances for each phase at each pore were used to calculate the pressure fields. Relative permeabilities were calculated during unsteady state flow and were compared to experimental coreflooding data. Although compositional, this model has some considerable limitations. The pressure determination in the pores is based solely on mass balances, not coupled with volume consistency equations and molar balance for each component. Also, free slip in the fluid-fluid interface is more suited for two-phase systems where the fluids have significantly different viscosities, and, finally, relative permeabilities were calculated during unsteady flow, where the outlet flow rates could be significantly different than inlet imposed flow rates. These drawbacks were addressed by Santos and Carvalho (2019). They have represented porous media as 2D regular grids of straight cylindrical capillaries, where the condensate and gas flow in annular configuration. The phases velocity profiles were obtained with a steady solution of Navier-Stokes equation. Molar balance equations coupled with volume consistency equations were solved at each time step, providing molar content and pressure for every pore. Local thermodynamic equilibrium was enforced in each pore and phase equilibrium calculations used the Peng and Robinson (1976) equation of state. Their work was limited to high capillary number regime and, consequently, did not include the formation of bridges of condensate in the capillaries nor capillary forces, which prevented the evaluation of the relative permeabilities dependency on flow rate and interfacial tension.

In this work, capillary pressure, more realistic network geometry and new pore-level phase distribution comprising the snap-off phenomenon are included in the compositional pore-network model presented by Santos and Carvalho (2019). With the proposed model, relative permeability curves for gas and condensate were generated for three different flow velocities and two interfacial tension values, and results showed good quantitative agreement with experimental data.

## 2. Pore-network Model

### 2.1. Pore-network Geometry

The pore-networks used in the present analysis consist of 3D structures of pores connected by circular constricted capillaries. Pores are identified by the index  $i$  and capillaries by the index  $j$ . The connectivity between them is mapped by an incidence matrix,  $\mathbf{C}$ , with elements defined as follows:

$$c_{ij} = \begin{cases} 0 & , \text{ if the capillary } j \text{ is not connected to the pore } i \\ -1 & , \text{ if the capillary } j \text{ enters the pore } i \\ +1 & , \text{ if the capillary } j \text{ exits the pore } i \end{cases}$$

Capillaries are characterized by a length  $L_j$  and a hyperbolic profile (eq. 1), with two geometric parameters, the maximum radius,  $R_{max,j}$  and the throat radius,  $R_{min,j}$ . Pores are defined by a control volume enclosing half the length of the capillaries contiguous to them, as illustrated in Figure 1.

$$r_j(x) = \sqrt{a_j + b_j x^2} \quad (1a)$$

$$a_j = R_{min,j}^2 \quad (1b)$$

$$b_j = \left(\frac{2}{L_j}\right)^2 (R_{max,j}^2 - R_{min,j}^2) \quad (1c)$$

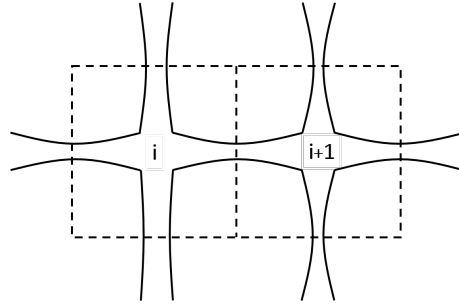


Figure 1: Definition of pore volume

The spacial configuration of pores and capillaries can be defined based on 3D pore-scale imaging of real rock samples, which leads to networks with variable capillary lengths and coordination number (number of capillaries connected to each pore). Alternatively, the network can be constructed based on 3D regular lattices, with realistic pore and throat size distributions, in the absence of more detailed petrophysical data.

## 2.2. Two-Phase Flow in the Capillaries

### 2.2.1. Flow Patterns Overview

For a gas condensate reservoir, the flow at pressures above the dew point pressure ( $P_{dp}$ ) contains only the gas phase (Fig.2a). If the pressure level is

lowered below the  $P_{dp}$ , however, a liquid phase emerges. It is considered in the model that the condensate wets completely the capillary walls (contact angle  $\theta \approx 0$ ) and tends to flow adjacent to them, developing an annular flow pattern (Fig.2b).

The annular flow in a capillary may be interrupted nonetheless, if the condensate film thickness ( $t$ ) reaches a critical value ( $t_{crit}$ ) above which the annular configuration becomes unstable. In this case, the liquid tends to evolve into a bridge accommodated at the capillary mid-section, in a phenomenon known as snap-off (Fig.2c). While a capillary accommodates a condensate bridge, the flow of gas and condensate is obstructed. After the snap-off, the flow can be reestablished if the pressure drop between the capillary extremities exceeds a critical capillary pressure value, and the liquid bridge is moved (Fig.2d).

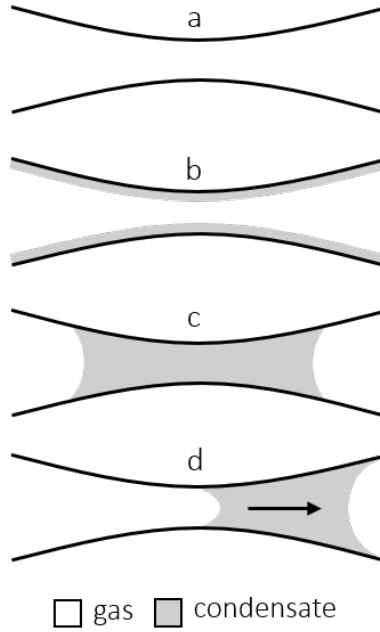


Figure 2: Evolution of condensate configuration in a throat

### 2.2.2. Gas and Condensate Annular Flow Conductances

The volumetric flow rate of gas and condensate in a capillary can be determined using the concept of fluid conductance:  $g = q/\Delta P$ , where  $\Delta P$  is the pressure difference in the capillary. The conductance calculations in this

model are based on the steady-state solution of the Navier-Stokes equation for a laminar two-phase annular flow in a straight capillary, given by equations 2 (Santos and Carvalho, 2019).

$$g_g = \frac{\pi}{8\mu_g L} (S_g R^2)^2 + \frac{\pi}{4\mu_l L} (R^2 - S_g R^2) S_g R^2 \quad (2a)$$

$$g_l = \frac{\pi}{8\mu_l L} (R^2 - S_g R^2)^2 \quad (2b)$$

In equations 2,  $\mu_g$  and  $\mu_l$  are the viscosities of the gas and liquid phases,  $S_g$  is the gas saturation and  $R$  and  $L$  are, respectively, the equivalent radius and length of the capillary. In order to adapt these conductances for constricted capillaries, an equivalent constant radius  $R$  was calculated for each capillary in the network.  $R$  represents the radius of a straight capillary that would yield the same volumetric flow rate as the constricted capillary, when subjected to the same pressure difference. The volumetric flow rate as a function of the pressure drop for a laminar, steady-state flow of a Newtonian fluid in an axisymmetric tube with hyperbolic profile Sochi (2013) was used, leading to the Equation 3 for the equivalent radius.

$$R = \left[ \frac{2R_{min}^3 R_{max}^2 \sqrt{R_{max}^2 - R_{min}^2}}{R_{min} \sqrt{R_{max}^2 - R_{min}^2} + R_{max}^2 \arctan \left( \sqrt{\frac{R_{max}^2 - R_{min}^2}{R_{min}^2}} \right)} \right]^{1/4} \quad (3)$$

### 2.2.3. Capillary Blocking Conditions

Several criteria for the formation of the condensate bridge in capillaries, in the context of pore-network modeling, have been suggested in the literature. These criteria are commonly highly simplified, so that the model computational effort is reduced. A condition based simply on a capillary radius threshold of  $20\mu m$  was adopted by Fang et al. (1996). Bustos and Toledo (2003) proposed a model containing square capillaries in which the condensate accumulation was initially contained in the capillary corners and the bridge of liquid was formed at condensate saturations greater than 21.4%. This value represents the condensate saturation at which the contact between the gas phase and the pore walls is lost. The same value was adopted by Momeni et al. (2017). Jamiolahmady et al. (2003b) suggested a criterion based on the time required for a bridge to be formed, as a function of the capillary geometry, fluid properties and initial condensate film thickness. In our

model, it was considered that a condensate bridge is formed upon reaching a critical condensate film thickness, proportional to the constriction radius of each capillary. Additionally, for the snap-off to happen, the geometry-controlled condition for the fluid break-up in constricted capillaries proposed by Beresnev et al. (2009) had to be met. This criterion, shown in Equation 4, reduces to the condition for the occurrence of the Plateau-Rayleigh instability in the limiting case of cylindrical capillaries.

$$L > 2\pi\sqrt{(R_{min} - t)(R_{max} - t)} \quad (4)$$

For  $t_{crit} = 0.25R_{min}$ , (which will be adopted in the analysis presented in this paper) the condensate saturations at which the snap-off occurs vary from  $\approx 1\%$ , for capillaries with very high  $R_{max}/R_{min}$  ratio, to 43.75%, for unconstricted capillaries. This interval is consistent with the values presented in the literature.

Once blocked, the critical pressure drop value for a capillary to be unobstructed is given by Equation 5. It is a function of the interfacial tension,  $\sigma$ , between the phases and the radii of the condensate bridge meniscii,  $R_1$  and  $R_2$ . The interfacial tension is calculated with the correlation proposed by Weinaug and Katz (1943), and the radii are related to the capillary geometry and the condensate saturation, as depicted in Figure 3.

$$\Delta P_{crit} = 2\sigma \left( \frac{1}{R_1} - \frac{1}{R_2} \right) \quad (5)$$

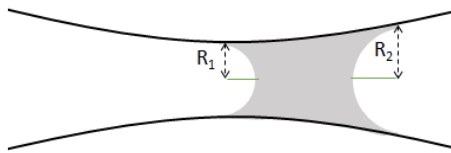


Figure 3: Condensate bridge radii,  $R_1$  and  $R_2$ , used to calculate  $\Delta P_{crit}$

The switch from opened to closed states in a capillary was implemented in the model by multiplying the conductances (eq. 2) by a continuous approximation of a unit step function  $H$ , presented in Appendix A.  $H$  is equal to unity, when the conditions for annular flow are met, and equal to zero, when the flow is blocked by a condensate bridge.

### 2.3. Equations Governing the Flow

Once the capillary conductances have been defined, the fluid content and pressure in the pores can be calculated. This is done via the coupled solution of Molar Balance Equations (section 2.3.1) and Volume Consistency Equations (section 2.3.2), along with the appropriate boundary conditions (section 2.3.3). The resulting system of non linear equations, described in section 2.3.4, relates the model variables,  $P_i$ ,  $N_i^k$  and  $s_i$ , respectively, the pressure and the number of moles of each component  $k$ , for all pores, and a source/sink term, for the pores located at the inlet/outlet of the network, and is solved using the Newton Raphson Method.

#### 2.3.1. Molar Balance Equation

The fluid content in a pore depends on the molar flow rates of the capillaries connected to it. Therefore, the molar balance equation (eq. 6) of each component  $k$  in a pore  $i$  is written in terms of the molar flow rate,  $\dot{n}_j^k$ , through its adjacent capillaries. Also, the term  $s_i^k$  is used for the pores located at the inlet and outlet of the network, to account for the molar flow through its boundaries. The molar flow in a capillary, given by Equation 7, converts the volumetric flow, calculated with the conductances and the pressure drop, into the molar flow, using the molar fraction of each component in the gas and liquid phases,  $y^k$  and  $x^k$ , and their molar densities,  $\xi_g$  and  $\xi_l$ . Equation 8 represents the pressure that drives the flow through the capillaries. It amounts to the difference in the pressures of the pores connected by the capillary, minus the interfacial pressure difference, when a condensate slug is formed. The inclusion of the interfacial pressure difference in eq. 8 is controlled by the function  $H^{int}$ , discussed in Appendix A.

$$\frac{\partial N_i^k}{\partial t} = - \sum_{j=1}^{n_{edge}} c_{ij} \dot{n}_j^k + s_i^k \quad (6)$$

$$\dot{n}_j^k = H_j (y^k \xi_g g_g + x^k \xi_l g_l)_j \Delta P_j \quad (7)$$

$$\Delta P_j = \sum_{m=1}^{n_{node}} c_{mj} P_m - H_j^{int} \Delta P_j^{int} \quad (8)$$

### 2.3.2. Volume Consistency Equation

In the proposed model, the pores contain only the gas and condensate phases. The volume of each pore, therefore, can be written as:  $V_i = V_i^g + V_i^l$ . Given that the network is slightly compressible, the pore volume can also be written as a function of the pore pressure and compressibility  $\nu_i = \frac{1}{\bar{V}_i} \frac{\partial V_i}{\partial P_i}$ .

Considering  $\bar{V}_i$  the volume of a pore at a reference pressure  $\bar{P}_i$ , its volume at any pressure can be approximated by Equation 9a. In regard to the pore contents,  $V_i^g + V_i^l$  can be determined by relating  $P_i$  and  $T$  with the fluid parameters  $\mathcal{L}_i$ ,  $Z_i^g$ ,  $Z_i^l$ ,  $x_i^k$  and  $y_i^k$  (respectively: the fraction of the  $N_i$  moles in the liquid phase, the compressibility factors and the molar fractions of each component  $k$  in the gas and liquid phases), as presented in Equation 9b.

$$V_i \approx \bar{V}_i [1 + \bar{\nu}_i (P_i - \bar{P})] \quad (9a)$$

$$V_i = N_i \left[ \mathcal{L}_i \left( \frac{Z_i^l RT}{P_i} - \sum_{k=1}^{n_c} v_k x_i^k \right) + (1 - \mathcal{L}_i) \left( \frac{Z_i^g RT}{P_i} - \sum_{k=1}^{n_c} v_k y_i^k \right) \right] \quad (9b)$$

The combination of the equations above leads to the volume consistency equation, given by Equation 10.

$$N_i - \frac{\bar{V}_i [1 + \bar{\nu}_i (P_i - \bar{P})]}{\mathcal{L}_i \left( \frac{Z_i^l RT}{P_i} - \sum_{k=1}^{n_c} v_k x_i^k \right) + (1 - \mathcal{L}_i) \left( \frac{Z_i^g RT}{P_i} - \sum_{k=1}^{n_c} v_k y_i^k \right)} = 0 \quad (10)$$

### 2.3.3. Boundary Conditions

Two sets of boundary conditions can be chosen for a flow analysis in the model. In the first, pressure is fixed at both inlet and outlet faces of the network, while in the second, molar flow rate is fixed at the inlet and pressure at the outlet. Other parameters that have to be imposed are the composition of the fluid injected in the network and the temperature.

### 2.3.4. Solution via Newton Raphson Method

Equations 6 and 10, associated with the appropriated boundary conditions, form the system of non-linear equations that relate the variables  $N_i^k$ ,  $P_i$  and  $s_i$  at each time step. The solution is obtained using Newton-Raphson method, where the unknown vector is  $\mathbf{u} = [N_i^k; P_i; s_i]$  and the residue vector

is  $\mathbf{R}=[(R_N)_i^k; (R_V)_i; (R_C)_i]$ . The entries of the vector  $\mathbf{R}$  are presented in equations 11.

$$(R_N)_i^k = (N_i^k)^{t+1} - (N_i^k)^t + dt \left\{ \sum_{j=1}^{n_{edge}} c_{ij} [H_j^\tau (y^k \xi_g g_g + x^k \xi_l g_l)^\tau_j \left( \sum_{m=1}^{n_{node}} c_{mj} P_m^{t+1} - H_j^{int,\tau} \Delta P_j^{int,\tau} \right) - z_{si}^{k\tau} s_i^{t+1}] \right\} \quad (11a)$$

$$(R_V)_i = (N_i)^{t+1} - \frac{\bar{V}_i [1 + \bar{v}_i (P_i^{t+1} - \bar{P})]}{\mathcal{L}_i^\tau \left( \frac{(Z_i^l)^\tau RT}{P_i^{t+1}} - \sum_{k=1}^{n_c} v_k (x_i^k)^\tau \right) + (1 - \mathcal{L}_i^\tau) \left( \frac{(Z_i^g)^\tau RT}{P_i^{t+1}} - \sum_{k=1}^{n_c} v_k (y_i^k)^\tau \right)} \quad (11b)$$

$$(R_C)_i = \begin{cases} \frac{dt (s_i - s_i^{imp})}{RT}, & \text{for imposed molar flow at node } i \\ \frac{(P_i - P_i^{imp}) \bar{V}_i}{RT}, & \text{for imposed pressure at node } i \end{cases} \quad (11c)$$

In order to reduce the computational effort, the phase equilibrium calculations are performed uncoupled from the system of equations 11. In these equations, when solving for  $\mathbf{u}^{t+1}$ , all the fluid properties dependent on the phase equilibrium calculations ( $x, y, \xi, g, \mathcal{L}, Z, H, \Delta P^{int}$ ) are computed with  $\mathbf{u}^\tau$ , where  $\tau$  corresponds to the preceding iteration of the Newton-Raphson method. In that way, instead of updating the phases saturations and properties only once per time-step, they are updated at every iteration between the solutions  $\mathbf{u}^{t+1}$  and  $\mathbf{u}^t$ , improving the accuracy of the uncoupled solution.

#### 2.4. Phase Equilibrium Calculations

For the phase equilibrium calculations, it is assumed constant temperature and local thermodynamic equilibrium at every time step within each pore. These calculations use a PT flash based on the Peng and Robinson (1976) cubic equation of state. Therefore, at every time step of a simulation, once  $P_i$  and  $N_i^k$  are evaluated, a flash calculation is performed for each pore  $i$  and new phase equilibrium conditions are determined. Details of the phase equilibrium calculations used in our model are described by Santos and Carvalho (2019).

### 3. Results

#### 3.1. Validation

Relative permeability ( $k_r$ ) curves obtained with coreflooding experiments by Jamiolahmady et al. (2003b) were used to validate the proposed model. The selected experiments were performed at three different gas flow rates and two different interfacial tension values, providing comprehensive data to evaluate whether the model is able to reproduce the effects of these parameters on gas and condensate coupled flow. Attempts to reproduce the same experiments with different pore-network models were presented by Jamiolahmady et al. (2003b) and Momeni et al. (2017). Their results were also used in the validation and discussion.

##### 3.1.1. Pore-network Construction

A Berea core sample with porosity  $\phi = 18.2\%$ , absolute permeability  $k = 92mD$  and irreducible water saturation  $S_{wc} = 26.4\%$  was used in the experiments Jamiolahmady et al. (2003b). For simulation purposes, we disregarded the presence of water and gas/condensate saturations were corrected in the results to be based on the total pore volume rather than the hydrocarbon pore volume. A Weibull probability distribution function of pore throat sizes was provided Jamiolahmady et al. (2003b) and used to define the constriction radius of the capillaries in the network. In this distribution, illustrated in Figure 4,  $R_{min}$  ranges from  $1.28\mu m$  to  $19.21\mu m$ , with an average value of  $8.5\mu m$ .

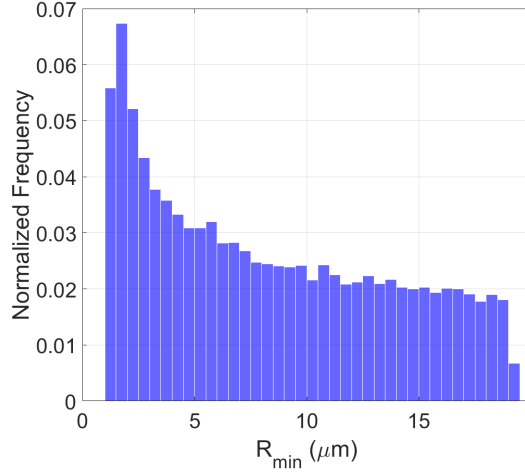


Figure 4: Normalized probability distribution function for  $R_{min}$

In their model, Jamiolahmady et al. (2003b) used constricted capillaries with a constant ratio  $R_{max}/R_{min} \approx 3.33$ . The authors suggested that this value did not reflect the true characteristics of the real porous medium and had been found to negatively affect the results. In the proposed model, this limitation was mitigated by calculating  $R_{max}$  values based on data of the aspect ratio between pore body and throat radii,  $AR = R_{max}/R_{min}$ , of a berea sample. This correction is important since the aspect ratio has a large impact on multi-phase flow simulation Dong (2008). The distribution function of the generated pore-network  $AR$ , along with that obtained for a pore-network extracted from a 3D Micro-CT image of a berea sample Dong (2008), is presented in Figure 5, indicating that values of  $AR$  used in our model are representative of Berea cores.

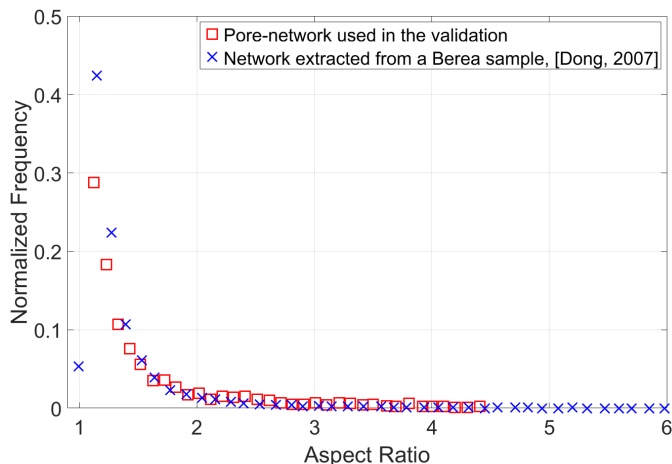


Figure 5: Aspect ratio of pore-networks extracted from a 3D image of a berea sandstone sample

A cubic lattice of  $20 \times 25 \times 25$  nodes represented the 3D spatial distribution of pores in the network. The coordination number was set to have an average value of 3, and was obtained by randomly removing capillaries from the original cubic lattice, as done in the previous network models Jamiolahmady et al. (2003b); Momeni et al. (2017). Additionally, the capillary length was chosen to be constant and equal to  $75 \mu m$ . This value was found to satisfy the necessity of matching  $\phi$  and  $k$ , with the set radii distribution, and also to be adequate to represent a berea sample Dong (2008).

### 3.1.2. Injected Fluid

Gas-condensate mixtures of methane ( $C1$ ) and normal butane ( $nC4$ ) were used as the fluid injected in the cores. The experiments were repeated at two levels of pressure, so that two different interfacial tension values were achieved. The pressures used in the simulations to reproduce the experimental conditions, for a fixed temperature of  $37^\circ C$ , as well as the viscosities of both phases calculated with the correlation proposed by Lohrenz et al. (1964), are presented in Table 1.

### 3.1.3. Gas and Condensate Flow Conditions

Each point of the  $k_r$  curves was measured by injecting the  $C1 - nC4$  mixture at a different condensate to gas flow ratio (CGR) in the cores. Also, for each CGR, the injected gas flow rate was controlled in order to generate gas flow velocities ( $v_g$ ) of  $9 md^{-1}$ ,  $18 md^{-1}$  and  $36 md^{-1}$ . This was reproduced

$\sigma$ (mN/m)	Pressure (MPa)	$\mu_g$ (Pa.s)	$\mu_l$ (Pa.s)
0.015	13.04	$2.26 \times 10^{-5}$	$3.51 \times 10^{-5}$
0.037	12.78	$2.14 \times 10^{-5}$	$3.71 \times 10^{-5}$

Table 1: Pressure and viscosities of gas and condensate at two interfacial tension values and 37°C

with the model by shifting the molar flow rate and molar fraction of the components in the injected composition. At a fixed pressure and temperature, reducing the fraction of methane in the mixture, while increasing appropriately the total molar flow rate, leads to higher CGRs for the same  $v_g$ . For the case at  $P_{out} = 13.04MPa$ , the C1 molar percentages were 75%, 77%, 78%, 79% and 79.5%, while for the case at  $P_{out} = 12.78MPa$  they were 75%, 78%, 79%, 80% and 80.5%. With these compositions, the initial condensate saturation in the networks ranged from 1% to 22% while the values achieved at steady-state flow varied from about 10% to 40%. The criteria for achieving steady-state in the model, which was necessary for the relative permeability predictions, were equal injected and produced molar flow rates, and constant average pressure and saturation in the network.

#### 3.1.4. Relative Permeability Curves

Figure 6 presents the relative permeability curves for gas and condensate phases,  $k_{rg}$  and  $k_{rc}$ , for  $\sigma = 0.037mN/m$  and  $v_g = 18md^{-1}$ . It shows the predictions of the proposed model, curves obtained with experiments Jamiolahmady et al. (2003b) and curves predicted with the pore-network models presented by Jamiolahmady et al. (2003b) and Momeni et al. (2017).

As discussed before, the model of Jamiolahmady et al. (2003b) does not consider the fluid composition and uses empirically adjusted coefficients to match the predictions to the measured relative permeabilities. Moreover, it assumes a fixed ratio between the pore body and pore throat radii. Although the model proposed by Momeni et al. (2017) uses a flash calculation to determine the amount of condensate at each throat, the system of equations is based on mass conservation in each pore and does not enforce molar conservation of each component. Also, in that work, the relative permeability curves are calculated in transient flow. At each time step, PT flash calculations are used to compute the volume of each phase in the throats and, consequently, the saturation in the network. The relative permeability of each phase is then calculated. This procedure leads to varying gas and condensate flow rates at

the outlet of the network during the simulation and does not represent the experimental procedure adopted in Jamiolahmady et al. (2003b) to measure the relative permeabilities.

All three models presented in the plot reproduce the experimental behavior of the gas relative permeability curve at low condensate saturation,  $S_c < 0.20$ . While ours and Momeni et al.'s results follow the measured  $k_{rg}$  curve up to  $S_c \approx 0.4$ , the predictions presented by Jamiolahmady et al. (2003b) present a sharp decline at  $S_c \approx 0.25$ , underpredicting the gas permeability for saturations higher than this value. Our model, while capturing the general behavior of the experimental  $k_{rc}$  curve, overestimates the value, particularly in the range  $0.15 \leq S_c \leq 0.35$ . This may be explained by the fact that the condensate conductance is calculated based on an annular flow pattern on smooth circular capillaries. Including the effect of wall roughness and non circular geometry can potentially reduce the mobility of the liquid phase and improve the results. Once again, the results from Jamiolahmady et al. (2003b) are accurate up to  $S_c = 0.25$ , above which they overpredict the experimentally measured  $k_{rc}$ . The curve presented by Momeni et al. (2017) does not capture the experimental curve behavior, with  $k_{rc} \approx 0$  for  $S_c < 0.17$  and a  $k_{rc}$  plateau for  $S_c > 0.30$ .

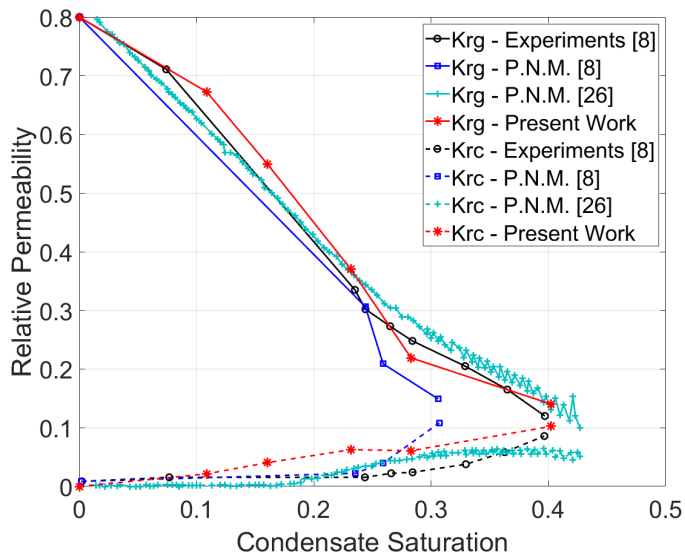


Figure 6:  $k_{rg}$  and  $k_{rc}$ , at  $\sigma = 0.037mN/m$  and  $v_g = 18md^{-1}$

The effect of gas velocity on the relative permeability curves is shown

in Figures 7 and 8. They represent the  $k_r$  curves for  $\sigma = 0.037mN/m$  and  $v_g$  equal to  $9md^{-1}$  and  $36md^{-1}$ , respectively. The proposed model is able to predict accurately the positive effect of flow rate on the relative permeability curves. For both gas velocities, our model produced results that more closely reproduce the experimental data than those presented by Jamiolahmady et al. (2003b). Momeni et al. (2017) did not present results for  $v_g$  other than  $18md^{-1}$  or for different values of interfacial tension in their model validation.

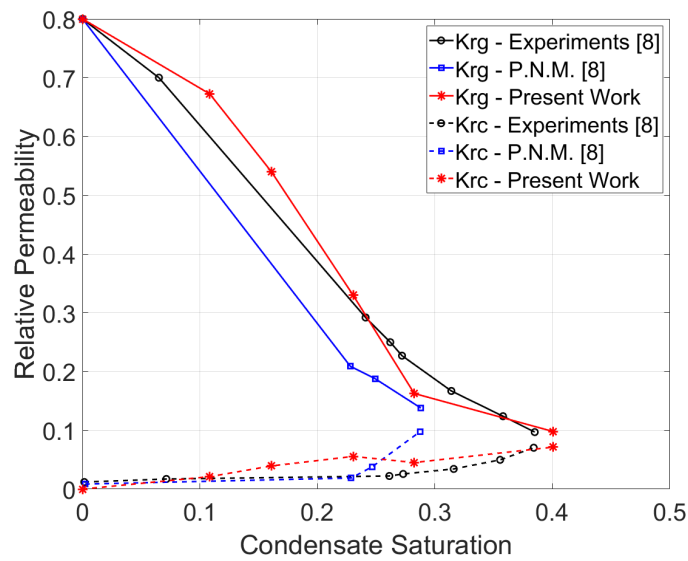


Figure 7:  $k_{rg}$  and  $k_{rc}$ , at  $\sigma = 0.037mN/m$  and  $v_g = 9md^{-1}$

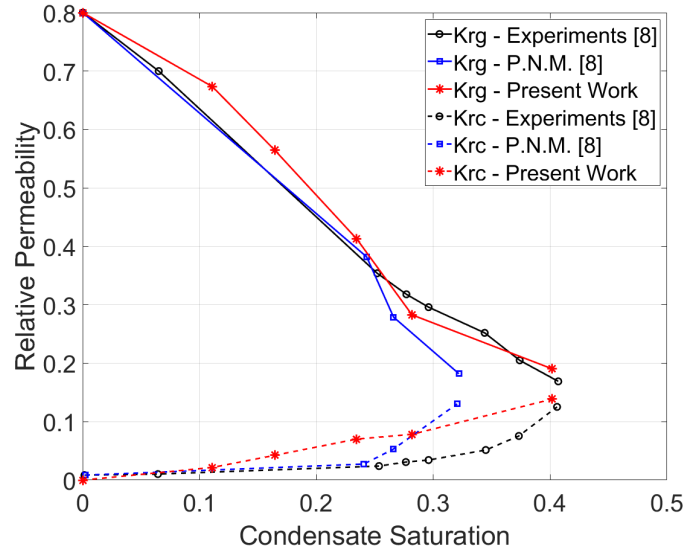


Figure 8:  $k_{rg}$  and  $k_{rc}$ , at  $\sigma = 0.037mN/m$  and  $v_g = 36md^{-1}$

The effect of interfacial tension on the flow behavior is presented in Figures 9, 10 and 11, which show the relative permeability curves at low interfacial tension,  $\sigma = 0.015mN/m$ , and different gas velocities. Higher  $k_r$  are expected at lower interfacial tension levels, as the phase trapping mechanism is weakened with reduced capillary pressure. This effect was both verified experimentally and predicted with the proposed model. For the three analyzed gas flow velocities, the predicted  $k_r$  curves agreed reasonably well with the measured data. While the model proposed by Jamiolahmady et al. (2003b) represented better the experimental  $k_r$  curves at  $v_g = 9md^{-1}$  and  $v_g = 18md^{-1}$ , their model had coefficients adjusted specifically to match the case at  $\sigma = 0.015mN/m$  and  $v_g = 9md^{-1}$ , leading to the almost perfect fit. The proposed model does not have any adjustable parameter to fit experimental data.

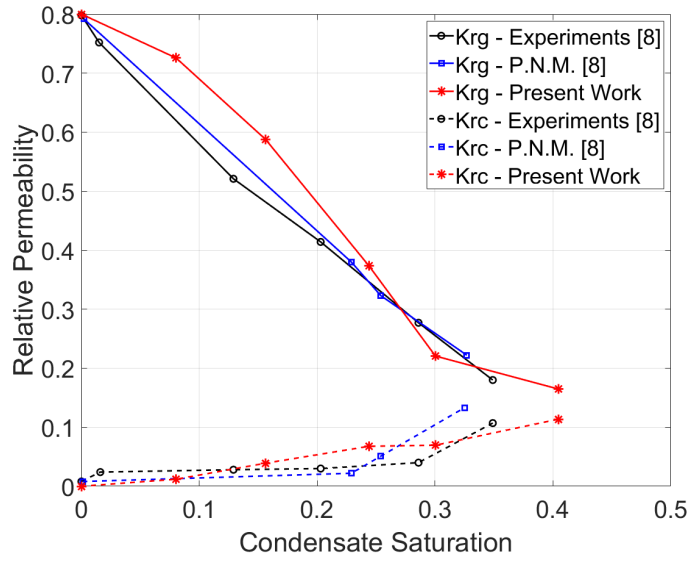


Figure 9:  $k_{rg}$  and  $k_{rc}$ , at  $\sigma = 0.015mN/m$  and  $v_g = 9md^{-1}$

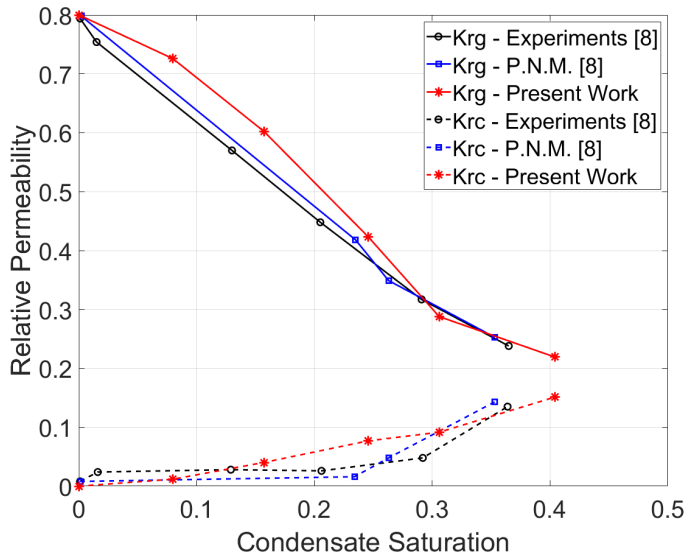


Figure 10:  $k_{rg}$  and  $k_{rc}$ , at  $\sigma = 0.015mN/m$  and  $v_g = 18md^{-1}$

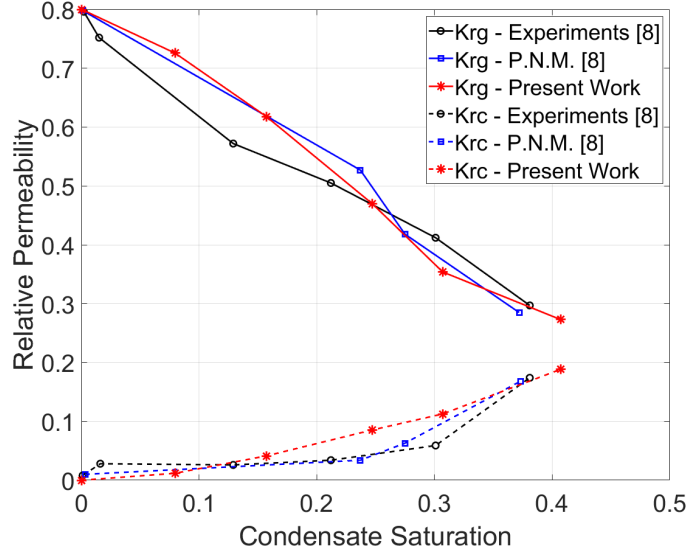


Figure 11:  $k_{rg}$  and  $k_{rc}$ , at  $\sigma = 0.015mN/m$  and  $v_g = 36md^{-1}$

### 3.2. Visualization of Blocked Capillaries

The sharp decline in  $k_{rg}$  with condensate saturation buildup in porous media has been attributed to the formation of condensate bridges that obstruct the gas flow in pore throats Al Harrasi et al. (2009); Coşkuner (1997); Jamiolahmady et al. (2000, 2003b). This phenomenon was well captured by our model, as illustrated in Figure 12. Figures 12 (a) to (e) show the opened and blocked capillaries of the network at the conditions used to construct the  $k_r$  curves at  $\sigma = 0.037mN/m$  and  $v_g = 18md^{-1}$ , displayed in Figure 6. For the two lowest  $S_c$  values, only a small fraction of capillaries is obstructed with condensate, 0.5% and 3.64%, for (a) and (b) respectively, meaning that  $k_{rg}$  is not significantly lessened. Also, at those saturation levels, the blocked capillaries not only are not numerous, but also are the most constricted ones, which implies that they provided a weak contribution to flow. For the three highest  $S_c$  values, the percentage of blocked capillaries rose to (c) 14.36%, (d) 43.50% and (e) 64.73%, which reduces significantly the available gas flowing paths, leading to a substantial decrease in  $k_{rg}$ .

### 3.3. Compositional Shift in Gas Condensate Flow

A compositional model based on molar conservation of each fluid component and phase equilibrium calculations can be used to study the changes in composition of each phase as they flow through a porous medium. As

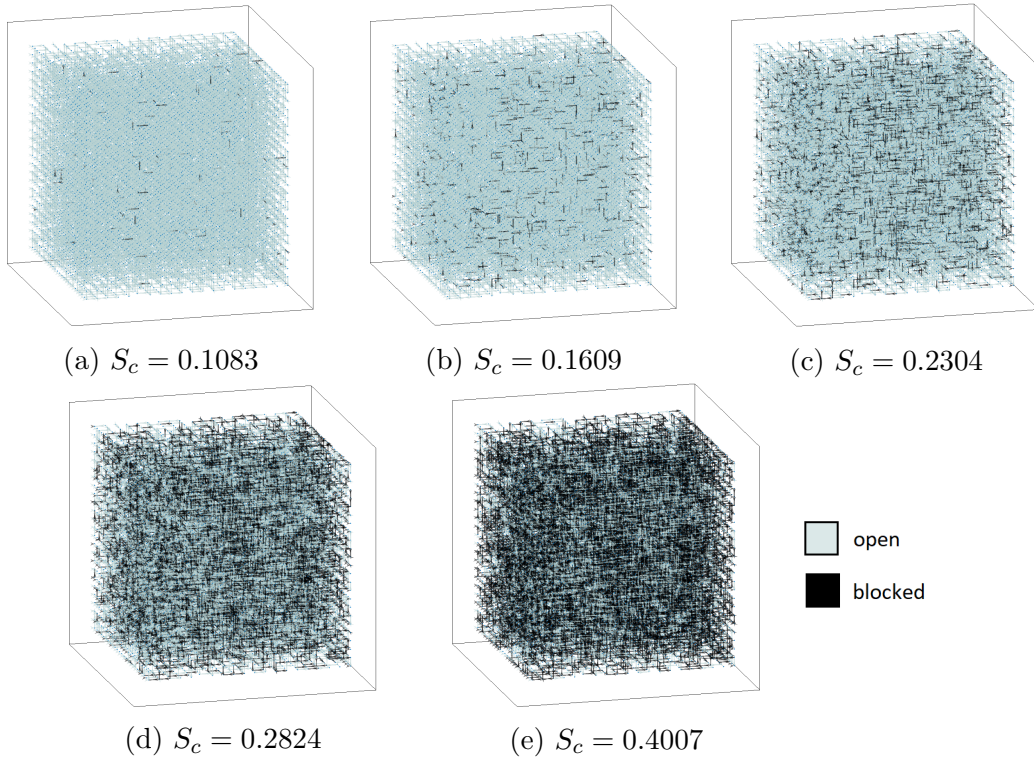


Figure 12: Blocked Capillaries, at  $\sigma = 0.037mN/m$  and  $v_g = 18md^{-1}$

the pressure in the network is lowered below the  $P_{dp}$ , the liquid phase that emerges is richer in heavier hydrocarbon components than the remaining gas phase. Since the flow of gas and liquid in small microchannels presents a large slip ratio, meaning that the gas velocity is higher than the condensate velocity Chung and Kawaji (2004); Kawahara et al. (2002); Kawaji and Chung (2004), this leads to an accumulation of liquid and, hence, heavy components in the porous media. This can be exemplified in Table 2. It contains the molar percentage of n-butane in the fluid injected in the network, and the molar percentage of the same component found in the network at steady-state condition, at  $\sigma = 0.037mN/m$  and  $v_g = 18md^{-1}$ .

For all injection scenarios, the fraction of  $nC4$ , the heavier component in the studied binary mixture, was higher in the network than in the injected fluid. Consequently, the  $C1 - nC4$  phase envelopes are displaced to the right, as illustrated in Figure 13, for the case where the  $nC4$  raised from 25% to 29.19%. This shift not only impacts the liquid dropout prediction, but also

<b>Injected <math>nC4\%</math></b>	<b><math>nC4\%</math> in the Network</b>
19.5	22.14
20.0	23.51
21.0	25.29
22.0	26.52
25.0	29.19

Table 2: Compositional shift in the network at at  $\sigma = 0.037mN/m$  and  $v_g = 18md^{-1}$

may lead to a transition in the general behavior of the mixture. It can be seen in the phase envelopes that the critical point, marked as a  $\Delta$ , was dislocated from  $T=33^\circ C$  to  $T=49^\circ C$ . Given that the network temperature was  $37^\circ C$ , this makes the behavior of the fluid mixture change from gas-condensate to volatile oil. This phenomenon, known to take place in gas condensate reservoirs near the wellbore region Roussenac (2001), impacts significantly the response of the fluid system to changes in pressure and temperature, and can only be appropriately predicted with compositional modeling, such as the one proposed here.

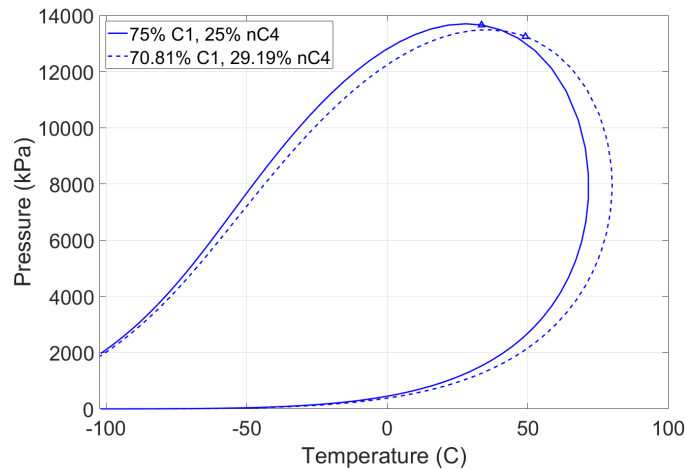


Figure 13: Phase Envelopes of a C1-nC4 binary mixture

#### 4. Conclusions

A new compositional dynamic pore-network model was presented to study gas and condensate coupled flow in porous media. The network comprised

a 3D structure of pores connected by constricted circular capillaries with hyperbolic profile. Gas and condensate conductances in the capillaries were calculated based on annular flow pattern, with liquid wetting capillary walls. Interruption of annular flow in the capillaries by the formation of condensate bridges was predicted, based on geometry and local liquid saturation. Once blocked, a capillary could be reopened if the pressure difference between its extremities exceeded a critical capillary pressure. Molar content and pressure in each pore were calculated through the solution of a system of non-linear equations with Newton-Raphson method, while the phases saturations were determined with a PT flash.

The model was validated by comparing predictions of steady-state gas and condensate relative permeability curves with experimental data available in the literature. Results demonstrated that the model represented well the effect of condensate saturation, interfacial tension and velocity on gas-condensate flow. Predicted  $k_r$  curves for flow at two different interfacial tension values and three different gas velocities demonstrated reasonable quantitative agreement with experimental data. Also, analyses of the fraction of blocked capillaries in the networks, for different condensate saturations, indicated that the formation and retention of condensate slugs in pore throats could constitute the main mechanism related to condensate banking.

The model also proved to be capable of predicting the buildup of heavy components in porous media during gas and condensate flow. For the  $C1 - nC4$  binary mixture used in the study, at all tested injection conditions, an increase of n-butane molar fraction was verified in the network. For the cases at high  $S_c$ , a transition in behavior from gas-condensate to volatile oil was observed.

With the provided evidence of predictive capability, we believe that the proposed model has potential to produce tailored data to large-scale gas-condensate reservoir simulation, based on specific reservoir rock, fluid composition, and flow conditions. This could lead to more realistic production estimations and benefit gas-condensate fields development planning. Future work in the model could encompass the implementation of wall roughness effect in condensate flow and the construction of more realistic pore-networks, generated based on pore-scale imaging techniques.

## 5. Acknowledgments

This research was funded by Repsol-Sinopec Brasil, under the RD&I Levy Fund Program of the National Petroleum Agency (ANP).

## Appendix A. Functions $H$ and $H^{int}$

Predicting whether a capillary is opened or closed to flow, due to the formation and retention of condensate bridges, constitutes a central part in the proposed model formulation. The flow status of a capillary, as available or not for flow, can be written as a function of its gas saturation and pressure difference. For relatively high  $S_g$  and/or high  $\Delta P$ , the capillary is opened to flow. The combination of low  $S_g$  and  $\Delta P$  leads to a capillary that is closed to flow. Including this transitions in the model would, therefore, make the conductances discontinuous function of  $S_g$  and  $\Delta P$ . Another instance of discontinuity in the model formulation involves the inclusion the interfacial pressure difference in the calculation of the capillary flow rate. This term only appears for low  $S_g$  and high  $\Delta P$ , meaning that a condensate slug is moving through the capillary.

However, as a condition for convergence of the multivariate Newton-Raphson method, the system of equations should contain only continuously differentiable functions in the neighborhood of its roots. Therefore, in order to avoid convergence issues, those discontinuous functions of  $S_g$  and  $\Delta P$  were substituted by the continuous approximations of unit step functions given by Equation A.1.

$$h_1 = \frac{1}{2} \left\{ 1 - \tanh \left[ \frac{1}{K_1} \left( \frac{S_g}{S_{g,crit}} - 1 \right) \right] \right\} \quad (\text{A.1a})$$

$$h_2 = \frac{1}{2} \left\{ 1 - \tanh \left[ \frac{1}{K_2} \left( \frac{\Delta P}{\Delta P_{crit}} - 1 \right) \right] \right\} \quad (\text{A.1b})$$

In Equation A.1,  $S_{g,crit}$  is the gas saturation calculated at a condensate film thickness  $t = t_{crit}$ . Thus,  $S_g < S_{g,crit}$  leads to the occurrence of snap-off. Function  $h_1$  is equal to one for  $S_g < S_{g,crit} - \epsilon$  and equal to zero for  $S_g > S_{g,crit} + \epsilon$ .  $2\epsilon$  is the thickness of the continuous representation region of the discontinuity of the step function.  $\Delta P_{crit}$  is the critical capillary pressure difference for a capillary to be reopened to flow, once the snap-off happened, given by eq. 5. Function  $h_2$  is equal to one for  $\Delta P < \Delta P_{crit} - \epsilon$  and equal

to zero for  $\Delta P > \Delta P_{crit} + \epsilon$ .  $K_1$  and  $K_2$  are shape factors that control the thickness  $2\epsilon$  on the transition region. Low values for  $K_1$  and  $K_2$  lead to smaller  $\epsilon$  and better approximations of a discrete step function, and their values should be adjusted according to functions  $h_1$  and  $h_2$  domains.

Since the capillary flow is interrupted when both  $S_g$  and  $\Delta P$  are below their critical values, the conductances were multiplied by  $H$ , given by equation A.2, in the capillary molar flow calculation (eq. 7).

$$H = 1 - h_1 h_2 \quad (\text{A.2})$$

As for the subtraction of the interfacial pressure drop in the capillary flow rate calculation, it was achieved by multiplying  $\Delta P^{int}$  by  $H^{int}$ , shown in Equation A.2.

$$H^{int} = h_1 - h_1 h_2 \quad (\text{A.3})$$

For the results presented in section 3, the adopted shape factors were  $K_1 = 0.1$  and  $K_2 = 0.3$ . This values were achieved upon successive trials of reducing the shape factors, and proved to be the low enough to represent well a unit step function, but not so low as to cause convergence difficulties.

## References

- Al Harrasi, M., Grattoni, C., Fisher, Q., Al-Hinai, S., 2009. Condensate displacement mechanisms in low permeability rocks, in: Proceedings, Society of Core Analysts. p. 15.
- Azin, R., Sedaghati, H., Fatehi, R., Osfouri, S., Sakhaei, Z., 2019. Production assessment of low production rate of well in a supergiant gas condensate reservoir: application of an integrated strategy. *Journal of Petroleum Exploration and Production Technology* 9, 543–560.
- Barnum, R., Brinkman, F., Richardson, T., Spillette, A., et al., 1995. Gas condensate reservoir behaviour: productivity and recovery reduction due to condensation, in: SPE annual technical conference and exhibition, Society of Petroleum Engineers.
- Beresnev, I.A., Li, W., Vigil, R.D., 2009. Condition for break-up of non-wetting fluids in sinusoidally constricted capillary channels. *Transport in porous media* 80, 581.

- Blunt, M.J., Bijeljic, B., Dong, H., Gharbi, O., Iglauer, S., Mostaghimi, P., Paluszny, A., Pentland, C., 2013. Pore-scale imaging and modelling. *Advances in Water resources* 51, 197–216.
- Bustos, C.I., Toledo, P.G., 2003. Pore-level modeling of gas and condensate flow in two-and three-dimensional pore networks: Pore size distribution effects on the relative permeability of gas and condensate. *Transport in Porous Media* 53, 281–315.
- Chen, H.L., Wilson, S.D., Monger-McClure, T.G., 1995. Determination of relative permeability and recovery for north sea gas condensate reservoirs, in: *SPE Annual Technical Conference and Exhibition*, Society of Petroleum Engineers.
- Chung, P.Y., Kawaji, M., 2004. The effect of channel diameter on adiabatic two-phase flow characteristics in microchannels. *International journal of multiphase flow* 30, 735–761.
- Coşkuner, G., 1997. Microvisual study of multiphase gas condensate flow in porous media. *Transport in Porous Media* 28, 1–18. doi:10.1023/A:1006505706431.
- Davarpanah, A., Mazarei, M., Mirshekari, B., 2019. A simulation study to enhance the gas production rate by nitrogen replacement in the underground gas storage performance. *Energy Reports* 5, 431–435.
- Dawe, R.A., Grattoni, C.A., 2007. Fluid flow behaviour of gas-condensate and near-miscible fluids at the pore scale. *Journal of Petroleum Science and Engineering* 55, 228–236. doi:10.1016/j.petro1.2006.08.009.
- Dong, H., 2008. Micro-CT imaging and pore network extraction. Ph.D. thesis. Department of Earth Science and Engineering, Imperial College London.
- El-Banbi, A.H., McCain Jr, W., Semmelbeck, M., et al., 2000. Investigation of well productivity in gas-condensate reservoirs, in: *SPE/CERI Gas Technology Symposium*, Society of Petroleum Engineers.
- Fang, F., Firoozabadi, A., Abbaszadeh, M., Radke, C., et al., 1996. A phenomenological modeling of critical condensate saturation, in: *SPE Annual Technical Conference and Exhibition*, Society of Petroleum Engineers.

- Henderson, G.D., Danesh, A., Tehrani, D.H., Al-Shaidi, S., Peden, J.M., et al., 1998. Measurement and correlation of gas condensate relative permeability by the steady-state method. *SPE Reservoir Evaluation & Engineering* 1, 134–140.
- Hoseinpour, S.A., Madhi, M., Norouzi, H., Soulgani, B.S., Mohammadi, A.H., 2019. Condensate blockage alleviation around gas-condensate producing wells using wettability alteration. *Journal of Natural Gas Science and Engineering* 62, 214–223.
- Jamiolahmady, M., Danesh, A., Henderson, G., Tehrani, D., et al., 2003a. Variations of gas-condensate relative permeability with production rate at near wellbore conditions: a general correlation, in: *Offshore Europe*, Society of Petroleum Engineers.
- Jamiolahmady, M., Danesh, A., Tehrani, D.H., Duncan, D.B., 2000. A mechanistic model of gas-condensate flow in pores. *Transport in porous media* 41, 17–46.
- Jamiolahmady, M., Danesh, A., Tehrani, D.H., Duncan, D.B., 2003b. Positive effect of flow velocity on gas-condensate relative permeability: network modelling and comparison with experimental results. *Transport in Porous Media* 52, 159–183.
- Joekar-Niasar, V., Hassanizadeh, S., 2012. Analysis of fundamentals of two-phase flow in porous media using dynamic pore-network models: A review. *Critical reviews in environmental science and technology* 42, 1895–1976.
- Kawahara, A., Chung, P.Y., Kawaji, M., 2002. Investigation of two-phase flow pattern, void fraction and pressure drop in a microchannel. *International journal of multiphase flow* 28, 1411–1435.
- Kawaji, M., Chung, P.Y., 2004. Adiabatic gas-liquid flow in microchannels. *Microscale Thermophysical Engineering* 8, 239–257.
- Li, K., Firoozabadi, A., et al., 2000. Phenomenological modeling of critical condensate saturation and relative permeabilities in gas/condensate systems. *Spe Journal* 5, 138–147.

- Lohrenz, J., Bray, B.G., Clark, C.R., et al., 1964. Calculating viscosities of reservoir fluids from their compositions. *Journal of Petroleum Technology* 16, 1–171.
- Mazarei, M., Davarpanah, A., Ebadati, A., Mirshekari, B., 2019. The feasibility analysis of underground gas storage during an integration of improved condensate recovery processes. *Journal of Petroleum Exploration and Production Technology* 9, 397–408.
- Mohammadi, S., Sorbie, K., Danesh, A., Peden, J., et al., 1990. Pore-level modelling of gas-condensate flow through horizontal porous media, in: *SPE Annual Technical Conference and Exhibition*, Society of Petroleum Engineers.
- Momeni, A., Dadvar, M., Hekmatzadeh, M., Dabir, B., 2017. 3d pore network modeling and simulation for dynamic displacement of gas and condensate in wellbore region. *International Journal of Multiphase Flow* 97, 147–156.
- Mott, R., Cable, A., Spearing, M., et al., 2000. Measurements and simulation of inertial and high capillary number flow phenomena in gas-condensate relative permeability, in: *SPE annual technical conference and exhibition*, Society of Petroleum Engineers.
- Nagarajan, N., Honarpour, M., Sampath, K., McMichael, D., 2004. Comparison of gas-condensate relative permeability using live fluid vs. model fluids. SCA2004-09 .
- Peng, D.Y., Robinson, D.B., 1976. A new two-constant equation of state. *Industrial & Engineering Chemistry Fundamentals* 15, 59–64. doi:10.1021/i160057a011.
- Roussenac, B., 2001. Gas Condensate Well Test Analysis. Master’s thesis. Stanford University. Stanford.
- Santos, M., Carvalho, M., 2019. Pore network model for retrograde gas flow in porous media. *Journal of Petroleum Science and Engineering* , 106635doi:https://doi.org/10.1016/j.petrol.2019.106635.
- Sochi, T., 2013. Newtonian flow in converging-diverging capillaries. *International Journal of Modeling, Simulation, and Scientific Computing* 4, 1350011. doi:10.1142/S1793962313500116.

- Wang, X., Mohanty, K., 1999. Critical condensate saturation in porous media. *Journal of colloid and interface science* 214, 416–426.
- Wang, X., Mohanty, K.K., et al., 2000. Pore-network model of flow in gas/condensate reservoirs. *SPE Journal* 5, 426–434.
- Weinaug, C.F., Katz, D.L., 1943. Surface tensions of methane-propane mixtures. *Industrial & Engineering Chemistry* 35, 239–246. doi:10.1021/ie50398a028.
- Zhang, A., Fan, Z., Zhao, L., 2020. An investigation on phase behaviors and displacement mechanisms of gas injection in gas condensate reservoir. *Fuel* 268, 117373.